PCCP

Accepted Manuscript

ROYAL SOCIETY OF CHEMISTRY

www.rsc.org/pccp

PCCP

Paper

Controlled Functionalisation of Single-Walled Carbon Nanotube Network Electrodes for the Enhanced Voltammetric Detection of Dopamine

Received 00th January 2015,
Accepted 00th January 2015

DOI: 10.1039/x0xx00000x

www.rsc.org/

Sharel P. E, Thomas S. Miller, Julie V. Macpherson* and Patrick R. Unwin*

Voltammetric studies of dopamine (DA) oxidation on pristine and acid-treated single-walled carbon nanotube (SWNT) network electrodes were undertaken in order to investigate both the effect of network density and acid treatment times on the voltammetric characteristics for DA oxidation and the susceptibility of the electrodes to fouling. Through careful control of catalysed chemical vapour deposition growth parameters, multiply interconnected and randomly oriented SWNT networks of two significantly different densities were grown (high density, HD, coverage >>10 μm length of SWNT per μm^{-2} and low density, LD, coverage = 5 (±1) μm_{SWNT} μm^{-2}). Acid treatment was performed to provide materials with different electrochemical properties and SWNT coverage, as determined by field emission-scanning electron microscopy, atomic force microscopy and micro-Raman spectroscopy. A high concentration of DA (100 μM) was deliberately employed to accelerate the fouling phenomenon associated with DA oxidation in order to evaluate the lifetime of the electrodes. HD pristine SWNT networks were found to promote more facile electron transfer (ET) and were less susceptible to blocking, compared to LD pristine SWNT networks. Acid treatment resulted in both a further enhancement of the ET rate and a reduction in susceptibility towards electrode fouling. However, lengthy acid treatment detrimentally affected ET, due to a decrease in network density and significant damage to the SWNT network structure. These studies highlight the subtle interplay between SWNT coverage and degree of acid functionalisation when seeking to achieve the optimal SWNT electrode for the voltammetric detection of DA.

Introduction

Dopamine (DA) is one of the most important catecholamine neurotransmitters in the human central nervous system and is widely studied in clinical research.[1, 2] Abnormal levels of DA can be an indicator of a neurological disorder; insufficient DA may be linked to a loss of neurons and can indicate Parkinson's disease, whereas schizophrenia is associated with elevated levels of DA in the prefrontal cortex.[2-4] The concentration of DA in the extracellular fluid of the caudate nucleus, which is involved in motor processes, is in the nM range for a person with Parkinson's disease, rising to ca. 0.01-1 μM for a healthy person.[5]

The early detection of abnormal DA concentration is critical and there has been significant investment in finding effective measurement methods at the levels required. Electrochemistry represents a very effective measurement methodology owing to the low cost, simplicity, short measurement times, and high sensitivity.[6] DA can be oxidised to dopamine-*o*-quinone, allowing the use of traditional electrochemical techniques for detection.[2, 7] However, the redox inactive decomposition products of DA oxidation, leucodopaminechrome and 5,6-dihydroxyindole, are known to adsorb on traditional metal or carbon electrodes, including electrodes formed from carbon nanotubes (CNTs),[8, 9] forming an insulating layer and leading to reduced stability and sensitivity. Electrode fouling will eventually lead to significant inhibition of electron transfer (ET) at the electrode surface.[10-12] The density of CNTs on the electrode surface has also been shown to play a role in the extent of electrode fouling.[13]

CNTs are a useful electrode material due to various promising physical[14] and chemical[15] properties, which include chemical stability,[16] biocompatibility,[14] low background currents,[17] good intrinsic electrical conductivity[18] and nanoscopic dimensions.[19] These properties make them promising for a wide range of applications in electrochemistry[15, 20, 21] and electroanalysis.[22] The use of CNTs as an electrode material in biological applications has attracted significant interest, particularly for the electrochemical detection of neurotransmitters.[2, 10, 23-26] The electrochemical detection of norepinephrine,[27] epinephrine,[28] serotonin,[10] and DA[10, 26, 29] have been reported. However, many of the aforementioned studies employed unpurified, as-grown CNTs synthesised using arc discharge, meaning that they were heavily contaminated with amorphous carbon[14] and metal nanoparticles (NPs).[30] The presence of these impurities has been shown to contribute to the electrochemical behaviour of the CNT electrodes.[14]

Department of Chemistry, University of Warwick, Coventry, CV4 7AL, UK.
E-mail: j.macpherson@warwick.ac.uk, p.r.unwin@warwick.ac.uk

CNT electrodes are often prepared by randomly dispersing CNTs onto a conducting electrode either by spin-coating or drop casting.[31, 32] There are a number of limitations associated with these CNT electrodes, including uneven CNT coverage[33] and electrochemical influence from the supporting substrate.[34] In contrast, the direct growth of single-walled CNTs (SWNTs) on *insulating substrates* using catalysed chemical vapour deposition (cCVD) allows the use of SWNTs as an electrode without the influence of the underlying substrate.[19] SWNTs grown using this method have also been shown to have a low defect density,[35] negligible amorphous carbon content and to be relatively free of catalytic NPs.[36]

The deliberate introduction of defects into CNTs may positively influence the electrochemical response towards "inner sphere" electrode reactions, for example, defects may create adsorption sites.[36, 37] Covalent functionalisation of SWNTs is a viable approach towards defect creation,[38-41] serving to change the surface hybridisation from sp^2 to sp^3,[3, 36] with the formation of surface functional groups such as carboxylic acids and alcohols.[41] For inner sphere DA oxidation, these groups have been postulated to act as catalytic sites,[36, 42] which enhance DA adsorption, as DA is protonated (*i.e.* positively charged) at physiological pH.[24] One simple method for creating defects in SWNTs is acid treatment, however the question as to the extent of acid treatment in relation to the density required for optimal electrochemical performance has not yet been fully addressed. In this work we investigate the effect of nitric acid treatment on both high density (HD) and low density (LD) SWNT network electrodes towards DA oxidation.

To negate the use of lithographic processing procedures, which can leave residue on the surface and therefore block potential sites for ET,[19] a micro-capillary electrochemical method (MCEM),[43, 44] is employed. Here, the electrochemical cell is formed by simply landing the meniscus of a solution-filled micro-capillary on the SWNT network electrode. This method allows multiple measurements to be made on the same surface in a combinatorial approach, simply by re-landing the capillary at different locations. This is extremely beneficial when investigating a redox process which may foul an electrode surface, especially when the electrode surface is not amenable to conventional electrode polishing in order to re-clean the surface, common with disposable-type electrodes. Here, the electrode can be refreshed simply by repositioning the capillary in a new spot on the substrate. By using this method we are able to investigate in detail the effect of SWNT density and level of SWNT functionalisation on DA electro-oxidation.

Experimental section

SWNT Network Growth

SWNT networks were grown on 2 cm × 2 cm Si/SiO_2 substrates (IDB Technologies Ltd., n-type, 525 µm thick with 300 nm of thermally grown SiO_2 on both sides) using cCVD. Fe[15] and Co[45] NPs were used as catalysts for the growth of LD and HD SWNT networks, respectively. Fe NPs were deposited by soaking the substrate in 1:100, ferritin (50-150 mg mL^{-1}, Aldrich) aqueous solution for 1 hour, followed by 2 min exposure to 100 W oxygen plasma (Emitech K1050X plasma asher). Co was deposited by sputtering (SC7640 sputter coater, Quorum Technologies Ltd., U.K.) at 1 kV for 20 s.

The cCVD procedure began with the substrate being heated from room temperature to 850 ^{o}C in 14 min under H_2 (BOC Gases, 99.95 %) atmosphere at a flow rate of 150 sccm, followed by stabilisation at 850 ^{o}C for 1 min. The growth of SWNT networks was initiated by bubbling Argon (Ar, BOC Gases, 99.9995 %) (850 sccm) through ethanol (EtOH) (Fisher, 99.99 %) held at 0 ^{o}C. Growth was carried out for 20 min. The system was allowed to cool under H_2 only.

Functionalisation of SWNT Networks

SWNT networks were treated with 3 M HNO_3 (70 %, Fisher) heated to 70 ^{o}C for 20, 120, 300, and 600 min. After removal from solution, the substrates were rinsed with distilled water and dried under N_2 gas before use. These medium strength acid treatments were employed to enable good control over the acid etching of SWNT networks and to avoid etching of the insulating substrate[36] compared to strong acid treatments[33] (concentrated H_2SO_4/HNO_3) which are typically employed to purify as-grown nanotubes. A similar medium acid treatment has been shown previously to oxidatively attack SWNTs.[46]

SWNT Networks Characterisation

SWNT networks were characterised using both field emission-scanning electron microscopy (FE-SEM, Zeiss Supra 55-VP, 1 kV acceleration voltage) and atomic force microscopy (AFM, tapping mode, Bruker-Nano Enviroscope). Micro-Raman spectra were recorded (Renishaw inVia Raman microscope; 514.5 nm Ar laser, 10 mW) with calibration against the Si peak (from the substrate) at 950 cm^{-1}. For each electrode, and after different treatments, three representative FE-SEM, AFM and micro-Raman measurements (n = 3) were recorded.

SWNT Electrode Fabrication and MCEM Setup

Electrical contact to the SWNT networks was achieved by evaporating Cr (3 nm) followed by Au (60 nm) through a shadow mask on the side of the Si/SiO_2 substrate using a Moorfield MiniLab deposition system (Moorfield Associates). Contact to the Au band was made via a Au pin. Neither came into contact with solution (Figure 1). To perform MCEM measurements, SWNT networks were mounted inside a humidity cell (de-aerated with N_2) and connected as a working electrode. The MCEM cell was formed from a borosilicate glass capillary (1.2 mm outer diameter, 0.69 mm internal diameter, Harvard Apparatus Ltd.), pulled to a small opening using a laser pipet puller (P-2000, Sutter Instrument Co.). The end was polished flat with an inner diameter of 50 µm (for DA detection) and 70 µm (for ferrocenylmethyltrimethylammonium ($FcTMA^+$) oxidation), and rendered hydrophobic through immersion in dichlorodimethylsilane (Fisher, ≥99 %) for 90 s, with Ar gas

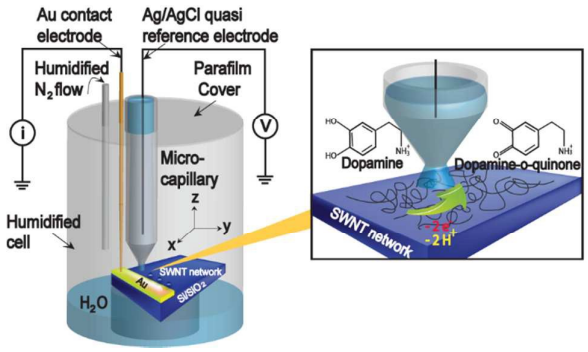

Fig. 1 Schematic of the experimental setup for the electro-oxidation of DA.

flowing through to prevent any internal silanisation. Next, the capillary was filled with the aqueous solution of interest and fitted with a AgCl-coated Ag wire quasi-reference/counter electrode (QRCE). The capillary was mounted on an *x-y-z* micropositioner (Newport 433 series) above the SWNT network substrate. With the aid of a camera (PixeLINK PL-B776U) the capillary was moved so that the meniscus landed on the SWNT network, without the capillary itself making contact to the electrode surface. Electrochemical measurements were made in the 2-electrode arrangement using a CH Instruments (Austin, TX; model 730A) potentiostat.

Chemicals and Solutions

All chemicals were used as received. Aqueous solutions were prepared using deionized water (resistivity of 18.2 MΩ cm at 25 ^{o}C). $FcTMA^+$ hexafluorophosphate was prepared in-house via metathesis of ferrocenylmethyltrimethylammonium iodide (Strem Chemical Co., 99 %) and silver hexafluorophosphate, $AgPF_6$ (Strem Chemical Co., 99.5 %). Potassium nitrate, KNO_3 (99 %) was purchased from Fisher. Dopamine hydrochloride was prepared in 0.01 M phosphate buffer aqueous solution (pH 7.4), and the pH was adjusted to 7.0 by adding 0.01 M citric acid (99.5 %, Sigma-Aldrich).[36] 100 µM DA was used throughout the experiments, as we were particularly interested in investigating potential blocking and/or fouling effects and this provides a reasonable concentration where such effects are 'accelerated'.[2, 47]

Results and discussion

Growth, Functionalisation and Characterisation of LD and HD SWNT Networks

Depending on their structure, SWNTs can be either metallic (mSWNT) or semiconducting (sSWNT).[48] In a randomly grown SWNT network, the ratio of mSWNTs to sSWNTs is approximately 1:3.[14] Hence, increasing the SWNT network density will change the electrical nature of the network resulting from increasing the number of mSWNT-mSWNT contacts. For all electrochemical studies the as-grown (pristine) SWNT network density was above the metallic percolation threshold.[36]

The FE-SEM and AFM images shown in Fig. 2a (i) and (ii), respectively, are of a typical pristine LD SWNT network; density in the range 4-6 $\mu m_{SWNT}\ \mu m^{-2}$. Similarly the FE-SEM and AFM images shown in Fig. 2b (i) and (ii), respectively, are of a pristine HD SWNT network which has a density of >>10 $\mu m_{SWNT}\ \mu m^{-2}$. It is difficult to determine the precise density as there are many SWNT bundles (evidenced by the apparent thicker widths in the AFM image) and several SWNT layers. Note that the SWNTs appear much broader in the FE-SEM images due to charging effects. Both networks have a connectivity much greater than the metallic percolation threshold ($\rho_{th(\text{metallic})}$), since $\rho_{th(\text{metallic})}$ is 1.4-2.4 $\mu m_{SWNT}\ \mu m^{-2}$ (based on typical SWNTs lengths, l, of 7-12 µm) and calculated from:[49]

$$\rho_{th(\text{metallic})} = 3\left[\frac{17.94}{l\pi}\right] \qquad (1)$$

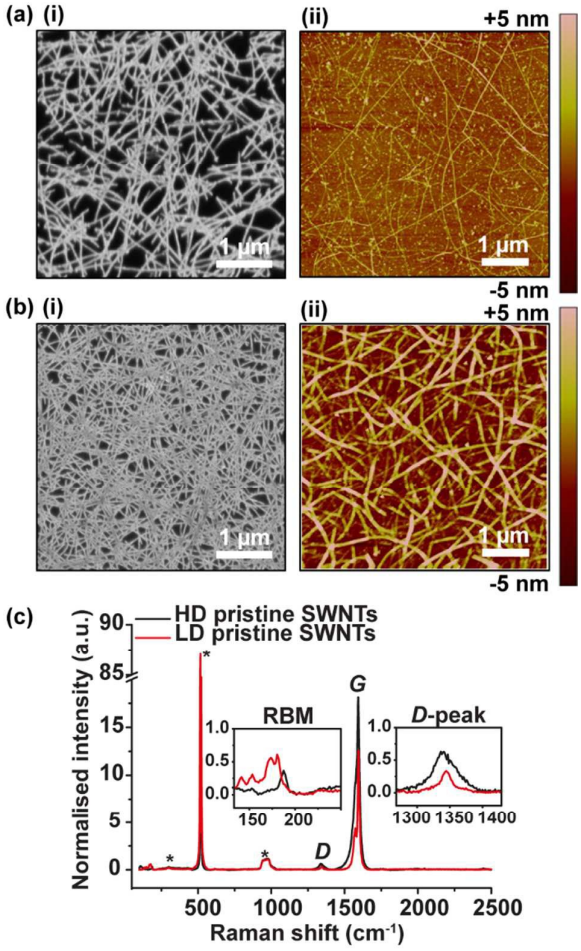

Fig. 2 Typical (i) FE-SEM and (ii) AFM images of (a) LD and (b) HD SWNT networks. (c) Corresponding micro-Raman spectra of LD (red) and HD (black) SWNT networks normalised to the Si/SiO_2 peak at 950 cm^{-1}.

Fig. 2c shows representative micro-Raman spectra of both HD and LD SWNT networks. The intensity of each spectrum was normalised with respect to the Si/SiO_2 peak at 950 cm^{-1}. The peaks marked with an (*) at 303 cm^{-1}, 521 cm^{-1}, and 950 cm^{-1} originate from the Si/SiO_2 substrate and provided a useful reference against which other peak intensities could be compared. In both spectra, the *G*-band (1565-1595 cm^{-1}) indicative of sp^2 carbon is clearly evident, containing a peak at 1595 cm^{-1} (G_p) and a shoulder, on the left-hand side, at 1574 cm^{-1}, due to mSWNT contributions.[50, 51] There are also radial breathing modes (RBM)[52] (100 to 350 cm^{-1}) present which also confirm that the networks consist of SWNTs. The HD SWNT network gave a higher relative intensity of the *G*-band due to the increased number of SWNTs in resonance with the Raman laser excitation.[52]

The *D*-peak at 1350 cm^{-1} originates from sp^3 carbon found at defects or in amorphous carbon deposits;[53] the intensity difference of the *G*-peak to that of the *D*-peak is often used as an indicator of the quality of SWNTs.[54] G_p was *ca*. 30 times the intensity of the *D*-peak for the HD SWNT networks and 40 times the intensity for the LD SWNT networks, showing that in both cases the as-grown pristine SWNTs were extremely clean and had low intrinsic defect densities and/or amorphous carbon content.

Representative FE-SEM and AFM images of LD and HD SWNT networks after exposure to 3 M HNO_3 at 70 °C for 20, 120, 300, and 600 min are shown in Fig. 3 and Fig. 4, respectively. It is clear from these images that the acid treatment acts to cut and shorten the SWNTs within the network, in line with previous reports where acid treatment has been shown to open tube ends,[14] and cut SWNTs.[39] The LD SWNT network density (Fig. 3) decreases from 4-6 μm_{SWNT} μm^{-2} for the pristine sample to (i) 3.8-5.2 μm_{SWNT} μm^{-2} after 20 min acid treatment, with further decreases to (ii) 3.7-4.7 μm_{SWNT} μm^{-2}, (iii) 3.3-4.3 μm_{SWNT} μm^{-2}, and (iv) 2.3-3.3 μm_{SWNT} μm^{-2} after 120 min, 300 min, and 600 min acid treatment, respectively.

It is important to note that as the length of SWNTs in the network becomes reduced, $\rho_{th(metallic)}$ is significantly increased. For example, from equation (1), $\rho_{th(metallic)}$ is calculated to be 1.7 μm_{SWNT} μm^{-2} when l = 10 µm, increasing to 8.6 μm_{SWNT} μm^{-2} when l = 2 µm. After 600 min acid treatment, the mean SWNT length in the LD SWNT networks had decreased to 1-4 µm (2.3-3.3 μm_{SWNT} μm^{-2}), meaning that the network density is now below $\rho_{th(metallic)}$ (4-17 μm_{SWNT} μm^{-2}), greatly jeopardising the ability of this material to function as an electrode material.[55] This highlights that functionalisation must be carefully undertaken, with due attention to the impact on the electronic properties of the SWNT network electrode.

The acid-treated HD SWNT networks (Fig. 4) show the same trend of reduced density with increasing acid treatment time as observed for the LD samples. Again, it can be seen how the SWNT network is acid etched, in particular in the AFM images in Fig. 4b, where it is evident that SWNTs have been cut into smaller fragments. Importantly, as the network density was significantly higher than the LD SWNT networks, even after lengthy 600 min acid treatments the network density remained reasonable, in the range 5.5-6.5 μm_{SWNT} μm^{-2} (Fig. 4b (iv)).

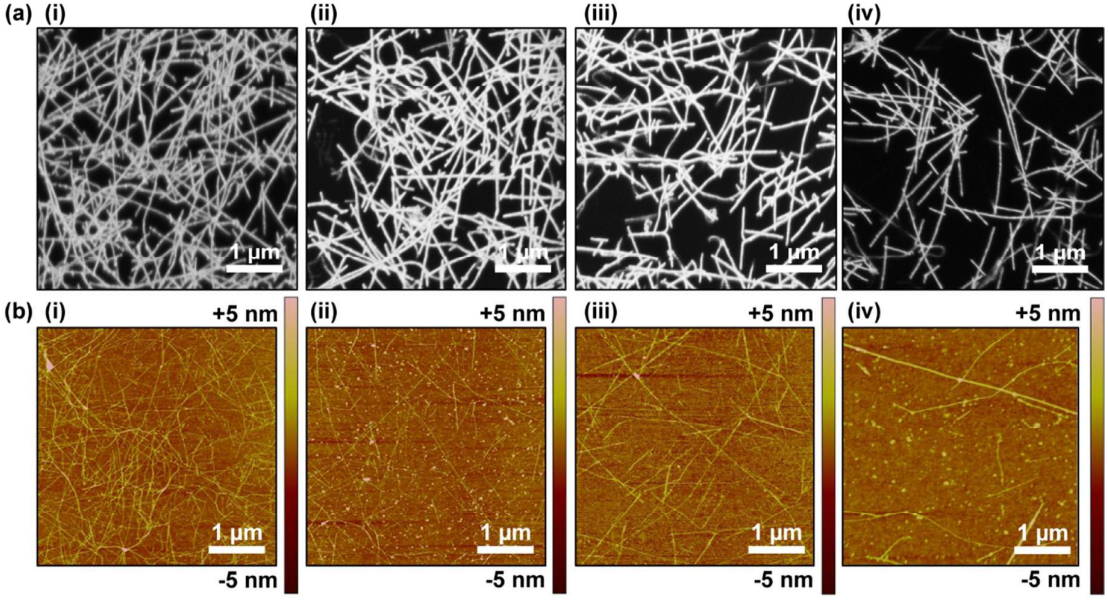

Fig. 3 Typical (a) FE-SEM and (b) AFM images of LD SWNT networks after (i) 20 min, (ii) 120 min, (iii) 300 min, and (iv) 600 min treatment with 3 M HNO_3 at 70 °C.

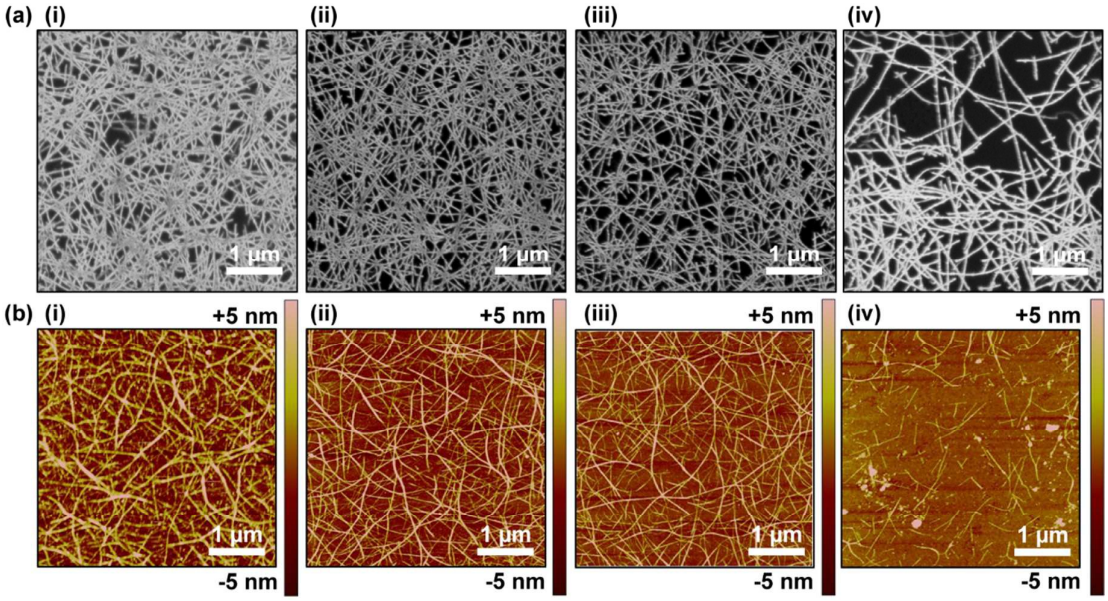

Fig. 4 Typical (a) FE-SEM and (b) AFM images of HD SWNT networks after (i) 20 min, (ii) 120 min, (iii) 300 min, and (iv) 600 min treatment with 3 M HNO_3 at 70 ^{o}C.

Typical micro-Raman spectra of HD and LD SWNT networks after different acid treatment times, focusing on the *D*- and *G*-bands, are shown in Fig. 5(a) and (b), respectively. The spectra in Figures 5a-c were normalised with respect to the intensity of Si at 950 cm^{-1}. To highlight relative changes in *G*-band intensity, the intensity of the *G*-band *vs.* acid treatment time is plotted as $i_{Gp\ (t)}/i_{Gp\ (pristine)}$ (Fig. 5c (i)), where *t* is the acid treatment time. The intensity of G_p, which is also indicative of SWNT network density (Fig. 2c), shows a decreasing $i_{Gp\ (t)}/i_{Gp\ (pristine)}$ signal with time, for both low and high density networks, as expected based on Figures 3 and 4. Specifically, for the HD sample, the intensity of G_p (Fig. 5c (i)) decreases to 96 %, 83 %, 78 %, and 72 % relative to the $G_{p\ (pristine)}$ intensity after 20, 120, 300, and 600 min acid treatment, respectively. The same scenario is apparent for LD SWNT samples, but with more severe changes in the intensity of G_p, which reduces to 83 %, 61 %, 40 %, and 18 % of $G_{p\ (pristine)}$, after 20, 120, 300, and 600 min acid treatment, respectively.

The intensity of the *D* peak with respect to i_{Gp} i.e. (i_D/i_{Gp}) is used for the evaluation of the defect density in SWNT networks.[56] The spectra were normalised to the G_p peak at 1595 cm^{-1} (Figures 5c (ii)) so that relative changes in *D*-band intensities were easily observed. It is apparent that the intensity of i_D/i_{Gp} in Fig. 5c (ii) increases with acid treatment time for both LD and HD SWNT networks as more defects are added to the SWNTs, during the etching and shortening of the SWNTs.

$FcTMA^+$ Oxidation

Before investigating the effect of SWNT network density and acid treatment on the oxidation of DA, preliminary studies were carried out using the one-electron outer sphere redox mediator (1 mM) $FcTMA^+$ in 100 mM KNO_3. The response of this mediator is unaffected by chemical changes to the surface of the SWNT.[37]

Fig. 6 shows cyclic voltammograms (CVs) for $FcTMA^+$ oxidation at (a) HD and (b) LD pristine SWNT networks before and after acid treatment with 3M HNO_3 at 70 ^{o}C for 20, 120, 300, and 600 min. All CVs for HD SWNT networks displayed fast ET with ΔE_p in the range 59 mV to 63 mV and peak currents (i_p) close to those expected for the oxidation of 1 mM $FcTMA^+$ at a planar disk electrode, as predicted by the Randles-Sevcik equation.[57] LD pristine SWNT networks after short acid treatment (20 min, 120 min, and 300 min) also showed fast ET with ΔE_p in the range of 59 mV, 64 mV, and 70 mV. These data are consistent with previous studies employing outer sphere redox couples, where SWNTs have been shown to support fast ET.[16, 19, 58-60] However, longer acid treatment of LD SWNT networks showed increased values of ΔE_p to 100 mV after 600 min acid treatment. The treatment lengths are sufficient to reduce the network density below the metallic percolation threshold, most likely resulting in an increased network resistance which produces ohmic drop effects in the CV response.

The data confirms that in all acid-treated cases of HD SWNT networks, the SWNT density is sufficiently high to achieve diffusional overlap between neighbouring SWNTs, with the electrode acting like a homogenous disk electrode with an equivalent geometry.[57, 61] It is also notable that for HD SWNT networks even after the 600 min acid exposure, the SWNT network has not become prohibitively resistive, despite the significant cutting of SWNTs.

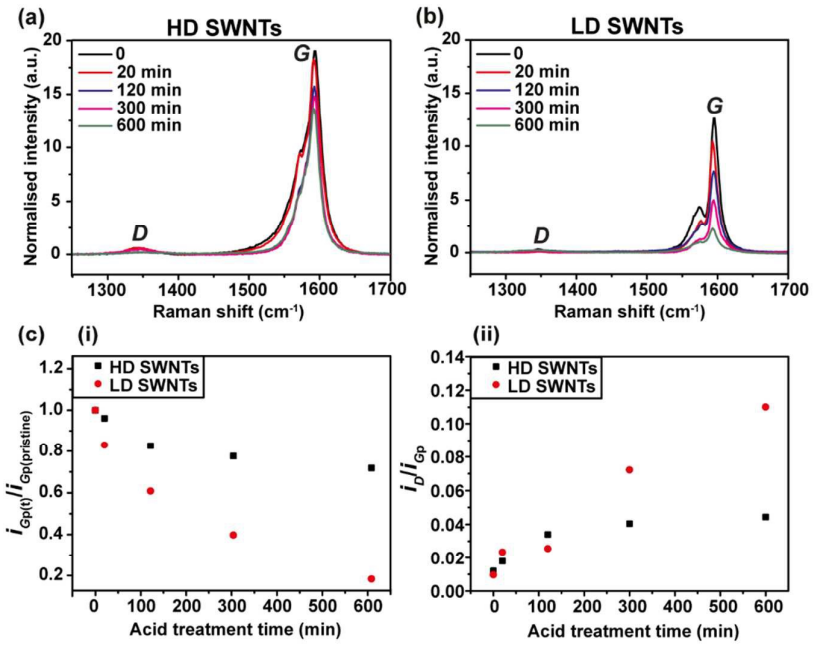

Fig. 5 Typical micro-Raman spectra of (a) HD and (b) LD SWNT networks before and after acid treatment, in 3 M HNO_3 at 70 °C for different times. (c) Effect of acid treatment time on (i) SWNT network density as expressed in the $i_{Gp\ (t)}/i_{Gp\ (pristine)}$ ratio and (ii) defect density as expressed in the i_D/i_{Gp} ratio for HD SWNT networks (black) and LD SWNT networks (red).

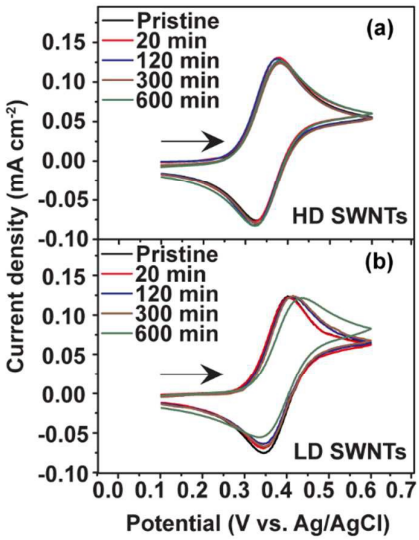

Fig. 6 Typical CVs for the oxidation of 1 mM $FcTMA^+$ in 100 mM KNO_3 (50 mV s^{-1}) at (a) HD and (b) LD pristine SWNT networks, and after 20 min, 120 min, 300 min, 600 min acid treatment in 3 M HNO_3 at 70 °C.

DA Detection

Fig. 7 shows the first cycle of a CV for the oxidation of 100 µM DA in 0.01 M citric acid pH 7.0 phosphate buffer at both HD and LD pristine SWNT networks. It is immediately apparent that the redox behaviour of DA is different on the SWNT networks of different densities, with the response on the HD SWNT networks showing a peak to peak separation (ΔE_p) of 508 ± 6 mV while the value of the LD SWNT networks is 591 ± 4 mV. This could be due to the higher surface coverage of the HD SWNT networks providing more sites for reaction, and/or the lower DA flux per SWNT length, also leading to less potential blocking.

Short time scale acid treatment, for 20 min, leads to a significant decrease in the peak to peak separation for DA oxidation by 140 mV for HD SWNT networks (ΔE_p = 368 mV) and by 100 mV for LD SWNT networks (ΔE_p = 491 mV). This means that the intrinsic ET kinetics (per unit length of SWNT) is more facile. This behaviour is attributed to acid treatment opening the end of the SWNTs and introducing functional groups, such as carboxylic acid,[33, 41] into the sidewall and at the ends of the opened SWNTs. These groups on the modified surface serve as potential sites for DA adsorption,[36, 42, 62] leading to enhanced overall apparent ET kinetics. It is also important to point out, however, that the apparently fast kinetics could be due to less susceptibility to blocking reactions, an aspect that we consider below.

As it is well-known that DA oxidation can lead to rapid fouling and blocking of the electrode surface, the extent of fouling on both HD and LD SWNT network electrodes was investigated by recording ten consecutive CVs as shown in Fig. 8a and b, respectively. It is obvious from Fig. 8b that the LD SWNT networks appear to be more susceptible to fouling than the HD SWNT networks (Fig. 8a), with a drop in the oxidative peak current, i_p by 20 % after ten CVs for the LD SWNT networks compared to an 8 % drop for the HD SWNT networks.

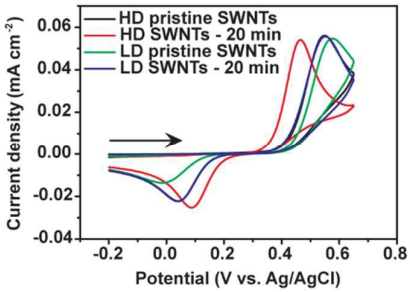

Fig. 7 CVs for the oxidation of 100 µM DA in 0.01 M citric acid pH 7.0 phosphate buffer (100 mV s^{-1}) at HD (black) and LD (green) pristine SWNT networks, and after 20 min acid treatment on HD (red) and LD (blue) SWNT networks.

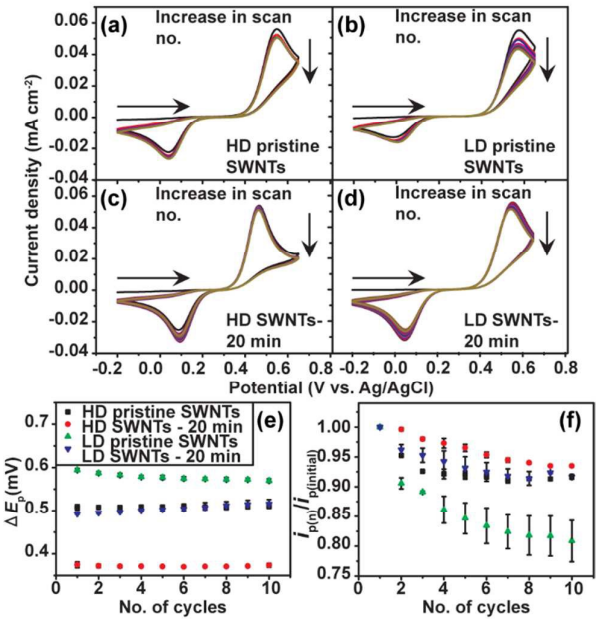

Fig. 8 Ten consecutive CVs, recorded at a scan rate of 100 mV s^{-1}, for the oxidation of 100 µM DA in 0.01 M citric acid pH 7.0 phosphate buffer at (a) HD and (b) LD pristine SWNT networks and 20 min acid-treated (c) HD and (d) LD SWNT network electrodes. Plot of (e) ΔE_p versus number of cycles (n = 3), and (f) $i_{p(n)}/i_{p(initial)}$ versus number of cycles (n = 3): HD (black) and LD (green) pristine SWNT networks, 20 min acid treatment on HD (red) and LD (blue) SWNT networks.

However, after just 20 min acid treatment, i_p falls by only 8.3 % for the LD SWNT networks (Fig. 8d), and 6.5 % for the HD SWNT networks (Fig. 8c), both after ten CV cycles. Summary data of ΔE_p and i_p normalised by the initial scan are shown in Fig. 8e and f (extracted from the data in Fig. 8a, b, c, and d), where $i_{p(n)}$ is the peak current per cycle number and "initial" indicates the first cycle.

It is apparent from the above studies that HD SWNT networks are superior for the detection of DA, showing faster apparent ET and little decrease in electrode performance, even after several cycles. These data also provide a reliable baseline, from which the effect of acid treatment on DA oxidation can be extracted. Based on these finding, we did not study further LD acid-treated SWNT networks but instead investigated the effect of acid treatment time on the DA electrochemical response of HD SWNT networks.

Fig. 9a shows CVs for the oxidation of 100 µM DA at pristine and acid-treated (3 M HNO_3, 70 °C) for 120, 300, and 600 min HD SWNT network electrodes, to see whether the performance towards DA detection could be optimised further. Three measurements were recorded for each experiment. 120 min acid-treated HD SWNT networks showed an even smaller ΔE_p of 353 ± 4 mV compared to pristine and 20 min acid treatment (Figure 7). However, after longer acid treatments, ΔE_p for DA oxidation increased, reaching 470 ± 12 mV and 598 ± 12 mV after 300 min and 600 min, respectively.

The studies with $FcTMA^+$ indicate that this is not due to the network increasing significantly in resistance. Rather, it indicates that there is an optimal balance required, trading off the creation of defects (functionalisation) of SWNTs which enhances the ET kinetics (and/or serves to inhibit blocking side-reactions), with the loss of active electrode material by etching, which reduces the overall fraction of active electrode area, placing stronger kinetic demands on the remaining material.

Fig. 10a, b, and c show repeat cycling CVs (ten cycles) for DA oxidation on HD SWNT networks treated with acid for times in the range 120 min to 600 min. Fig. 10d shows summary data for ΔE_p as a function of treatment time and number of CV cycles. It can be seen that ΔE_p remains relatively stable over ten consecutive scans for all acid-treated networks, even after lengthy acid treatments. However, i_p decreases with each consecutive scan (Fig. 10e), with the extent depending on the acid treatment conditions (and hence SWNT coverage). i_p is reduced by 6.5 % after 20 min acid treatment (Fig. 8c), falling to 5.5 % after 120 min (Fig. 10a) (after ten scans for each). However, longer acid treatment on SWNT networks caused i_p to fall by 13 % and 22 % for 300 and 600 min (after ten scans), respectively, indicating that these treatment lengths are sufficient to reduce the network density enough to create a fouling effect similar to that of LD SWNT networks (Fig. 8b).

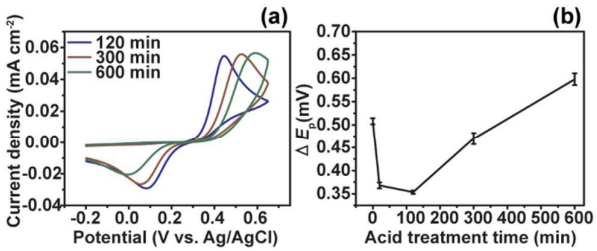

Fig. 9 (a) CVs for the oxidation of 100 µM DA, recorded at a scan rate of 100 mV s^{-1}, in 0.01 M citric acid pH 7.0 phosphate buffer (100 mV s^{-1}) at HD SWNT networks after acid treatment for 120 min (blue), 300 min (brown), and 600 min (green) with 3 M HNO_3 at 70 °C; (b) plot of ΔE_p versus acid treatment times (n = 3).

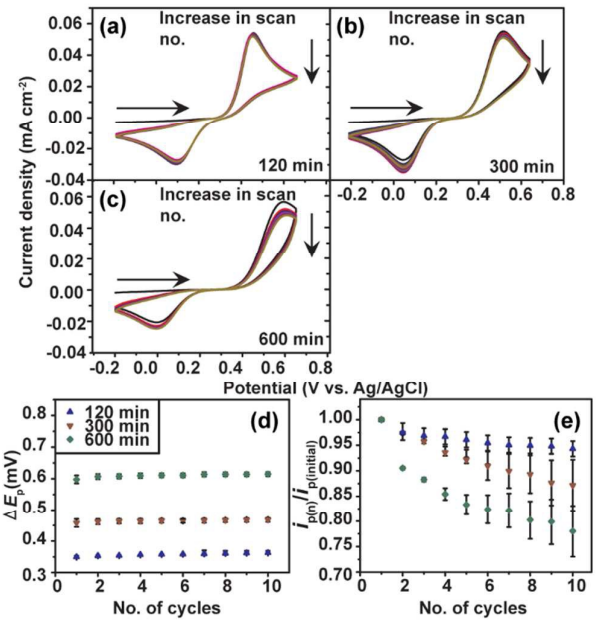

Fig. 10 Ten consecutive CVs, recorded at a scan rate of 100 mV s^{-1}, for the oxidation of 100 μM DA in 0.01 M citric acid pH 7.0 phosphate buffer with acid treatment times of: (a) 120 min, (b) 300 min, and (c) 600 min. Plot of (d) ΔE_p versus number of cycles (n = 3) and (e) $i_{p(n)}/i_{p(initial)}$ versus number of cycles (n = 3): HD SWNT networks after different acid treatment times of 120 min, 300 min, and 600 min.

For this study, we show that a 120 min acid treatment on a HD SWNT network is optimum for maximising ET and minimising electrode fouling. These data also highlight that there is a subtle interplay of acid treatment and overall SWNT coverage (intrinsic and after acid treatment) on both the ET kinetics and blocking effects that need to be taken into account to produce the optimal SWNT network electrode for DA detection.

Conclusions

This work has shown that chemical acid treatment paves the way for the preparation of functionalised SWNT networks, which enhance the ET characteristics for the oxidation of the neurotransmitter DA. It has also been demonstrated that it is essential that the advantages brought by acid treatment are not offset by adversely decreasing the density of SWNT networks. Hence, a balance must be struck between chemical treatment and overall SWNT coverage to optimise the performance of SWNT electrodes. The local combinatorial approach outlined herein provides a route to screening and identifying the best conditions for DA detection.

Both LD and HD SWNT network electrodes were successfully obtained by cCVD growth. HD SWNT networks exhibit more facile ET for DA oxidation and are less susceptible to blocking, owing to more active surface area over the same geometrical area, leading to a lower flux (mass transport) per unit length of SWNT. It was found that a controlled (120 min) acid treatment significantly improved the apparent oxidation kinetics of DA (and/or less electrode blocking), as manifested by a decrease in ΔE_p. Repetitive CV cycling confirmed that acid-treated SWNT networks suffered much less from the effects of surface blocking, with i_p only reducing by 5.5 % over ten cycles (HD SWNT networks). However, longer acid treatments (300 and 600 min) caused SWNTs to cut and etch too much which adversely affected the overall response.

The SWNT configuration we use involving a sparse arrangement on an insulating support, differs greatly from the usual use of SWNTs in electrochemistry.[14] The arrangement we adopt is beneficial in enhancing detection limits,[63] due to the very low background current of the network. The studies herein further enhance the capability of this type of arrangement by showing how SWNT networks can be tailored to perform a particular function. The MCEM is a particularly attractive means of quickly assessing the impact of functionalisation and is expected to find wider use in electrochemistry.

Acknowledgements

S.P.E. would like to thank the University of Warwick for funding through the award of the Chancellor's International Scholarship. T.S.M. acknowledges support from (EPSRC) for funding and award of a DTA studentship. This work was in part supported by a European Research Council award (ERC-2009-AdG 247143-QUANTIF) to P.R.U. The authors thank Aleix G. Güell and Robert A. Lazenby for fruitful discussions.

References

1 F. Gao, X. Cai, X. Wang, C. Gao, S. Liu, F. Gao and Q. Wang, *Sensor Actuat. B-Chem.*, 2013, **186**, 380-387.
2 A. N. Patel, S. -Y. Tan, T. S. Miller, J. V. Macpherson and P. R. Unwin, *Anal. Chem.*, 2013, **85**, 11755-11764.
3 C. B. Jacobs, M. J. Peairs and B. J. Venton, *Anal. Chim. Acta*, 2010, **662**, 105-127.
4 Z. A. Alothman, N. Bukhari, S. M. Wabaidur and S. Haider, *Sensor Actuat. B-Chem.*, 2010, **146**, 314-320.
5 B. J. Venton and R. M. Wightman, *Anal. Chem.*, 2003, **75**, 414-421.
6 M. N. Zhang, K. P. Gong, H. W. Zhang and L. Q. Mao, *Biosens. Bioelectron.*, 2005, **20**, 1270-1276.
7 S. Alwarappan, K. S. A. Butcher and D. K. Y. Wong, *Sensor Actuat. B-Chem.*, 2007, **128**, 299-305.
8 A. G. Güell, K. E. Meadows, P. R. Unwin and J. V. Macpherson, *Phys. Chem. Chem. Phys.*, 2010, **12**, 10108-10114.
9 A. N. Patel, K. McKelvey and P. R. Unwin, *J. Am. Chem. Soc.*, 2012, **134**, 20246-20249.
10 B. E. K. Swamy and B. J. Venton, *Analyst*, 2007, **132**, 876-884.
11 H. Zhao, Y. Z. Zhang and Z. B. Yuan, *Analyst*, 2001, **126**, 358-360.
12 F. Bernsmann, J. C. Voegel and V. Ball, *Electrochim. Acta*, 2011, **56**, 3914-3919.
13 I. Dumitrescu, J. P. Edgeworth, P. R. Unwin and J. V. Macpherson, *Adv. Mater.*, 2009, **21**, 3105-3109.

14 I. Dumitrescu, P. R. Unwin and J. V. Macpherson, *Chem. Commun.*, 2009, **45**, 6886-6901.
15 P. V. Dudin, P. R. Unwin and J. V. Macpherson, *J. Phys. Chem. C*, 2010, **114**, 13241-13248.
16 A. G. Güell, N. Ebejer, M. E. Snowden, K. McKelvey, J. V. Macpherson and P. R. Unwin, *P. Natl. Acad. Sci. USA*, 2012, **109**, 11487-11492.
17 A. Rutkowska, T. M. Bawazeer, J. V. Macpherson and P. R. Unwin, *Phys. Chem. Chem. Phys.*, 2011, **13**, 5223-5226.
18 I. Dumitrescu, P. V. Dudin, J. P. Edgeworth, J. V. Macpherson and P. R. Unwin, *J. Phys. Chem. C*, 2010, **114**, 2633-2639.
19 I. Heller, J. Kong, H. A. Heering, K. A. Williams, S. G. Lemay and C. Dekker, *Nano Lett.*, 2005, **5**, 137-142.
20 T. M. Day, P. R. Unwin, N. R. Wilson and J. V. Macpherson, *J. Am. Chem. Soc.*, 2005, **127**, 10639-10647.
21 G. G. Wildgoose, C. E. Banks and R. G. Compton, *Small*, 2006, **2**, 182-193.
22 J. J. Gooding, *Electrochim. Acta*, 2005, **50**, 3049-3060.
23 S. B. Hocevar, J. Wang, R. P. Deo, M. Musameh and B. Ogorevc, *Electroanal.*, 2005, **17**, 417-422.
24 J. Zhao, W. Zhang, P. Sherrell, J. M. Razal, X. F. Huang, A. I. Minett and J. Chen, *ACS Appl. Mater. Inter.*, 2012, **4**, 44-48.
25 H. Bi, Y. Li, S. Liu, P. Guo, Z. Wei, C. Lv, J. Zhang and X. S. Zhao, *Sensor Actuat. B-Chem.*, 2012, **171**, 1132-1140.
26 P. J. Britto, K. S. V. Santhanam and P. M. Ajayan, *Bioelectroch. Bioener.*, 1996, **41**, 121-125.
27 J. X. Wang, M. X. Li, Z. J. Shi, N. Q. Li and Z. N. Gu, *Electroanal.*, 2002, **14**, 225-230.
28 F. Valentini, G. Palleschi, E. L. Morales, S. Orlanducci, E. Tamburri and M. L. Terranova, *Electroanal.*, 2007, **19**, 859-869.
29 G. A. Rivas, M. D. Rubianes, M. C. Rodriguez, N. E. Ferreyra, G. L. Luque, M. L. Pedano, S. A. Miscoria and C. Parrado, *Talanta*, 2007, **74**, 291-307.
30 C. E. Banks, A. Crossley, C. Salter, S. J. Wilkins and R. G. Compton, *Angew. Chem. Int. Edit*, 2006, **45**, 2533-2537.
31 H. X. Luo, Z. J. Shi, N. Q. Li, Z. N. Gu and Q. K. Zhuang, *Anal. Chem.*, 2001, **73**, 915-920.
32 D. Paolucci, M. Marcaccio, C. Bruno, F. Paolucci, N. Tagmatarchis and M. Prato, *Electrochim. Acta*, 2008, **53**, 4059-4064.
33 M. W. Marshall, N. S. Popa and J. G. Shapter, *Carbon*, 2006, **44**, 1137-1141.
34 J. Zhao, Y. Yu, B. Weng, W. Zhang, A. T. Harris, A. I. Minett, Z. Yue, X. Huang and J. Chen, *Electrochem. Commun.*, 2013, **37**, 32-35.
35 Y. W. Fan, B. R. Goldsmith and P. G. Collins, *Nat. Mater.*, 2005, **4**, 906-911.
36 I. Dumitrescu, N. R. Wilson and J. V. Macpherson, *J. Phys. Chem. C*, 2007, **111**, 12944-12953.
37 T. S. Miller, J. V. Macpherson and P. R. Unwin, *Phys. Chem. Chem. Phys.*, 2014, **16**, 9966-9973.
38 M. Lurlo, D. Paolucci, M. Marcaccio and F. Paolucci, *Chem. Commun.*, 2008, **40**, 4867-4874.
39 J. J. Gooding, A. Chou, J. Liu, D. Losic, J. G. Shapter and D. B. Hibbert, *Electrochem. Commun.*, 2007, **9**, 1677-1683.
40 A. Chou, T. Bocking, N. K. Singh and J. J. Gooding, *Chem. Commun.*, 2005, **7**, 842-844.
41 K. Flavin, I. Kopf, E. D. Canto, C. Navio, C. Bittencourt and S. Giordani, *J. Mater. Chem.*, 2011, **21**, 17881-17887.
42 S. H. DuVall and R. L. McCreery, *J. Am. Chem. Soc.*, 2000, **122**, 6759-6764.
43 T. M. Day, P. R. Unwin and J. V. Macpherson, *Nano Lett.*, 2007, **7**, 51-57.
44 T. S. Miller, S. Sansuk, S. P. E, S. C. S. Lai, J. V. Macpherson and P. R. Unwin, *Catal. Today*, 2014, **244**, 136-145.
45 P. V. Dudin, P. R. Unwin and J. V. Macpherson, *Phys. Chem. Chem. Phys.*, 2011, **13**, 17146-17152.
46 B. R. Azamian, K. S. Coleman, J. J. Davis, N. Hanson and M. L. H. Green, *Chem. Commun.*, 2002, **4**, 366-367.
47 A. N. Patel, P. R. Unwin and J. V. Macpherson, *Phys. Chem. Chem. Phys.*, 2013, **15**, 18085-18092.
48 A. F. Holloway, K. Toghill, G. G. Wildgoose, R. G. Compton, M. A. H. Ward, G. Tobias, S. A. Llewellyn, B. Ballesteros, M. L. H. Green and A. Crossley, *J. Phys. Chem. C*, 2008, **112**, 10389-10397.
49 L. Hu, D. S. Hecht and G. Gruner, *Nano Lett.*, 2004, **4**, 2513-2517.
50 C. M. Yang, J. S. Park, K. H. An, S. C. Lim, K. Seo, B. Kim, K. A. Park, S. Han, C. Y. Park and Y. H. Lee, *J. Phys. Chem. B*, 2005, **109**, 19242-19248.
51 J. Li, Y. Huang, P. Chen and M. B. Chan-Park, *Chem. Mater.*, 2013, **25**, 4464-4470.
52 M. S. Dresselhaus, G. Dresselhaus, A. Jorio, A. G. Souza and R. Saito, *Carbon*, 2002, **40**, 2043-2061.
53 V. Skakalova, A. B. Kaiser, W. U. Dettlaff, K. Hrncarikova and S. Roth, *J. Phys. Chem. B*, 2005, **109**, 7174-7181.
54 A. Jorio, R. Saito, G. Dresselhaus and M. S. Dresselhaus, *Philos. T. Roy. Soc. A*, 2004, **362**, 2311-2336.
55 J. P. Edgeworth, N. R. Wilson and J. V. Macpherson, *Small*, 2007, **3**, 860-870.
56 M. S. Dresselhaus, A. Jorio, A. G. Souza Filho and R. Saito, *Philos. T. Roy. Soc. A*, 2010, **368**, 5355-5377.
57 P. Bertoncello, J. P. Edgeworth, J. V. Macpherson and P. R. Unwin, *J. Am. Chem. Soc.*, 2007, **129**, 10982-10983.
58 T. S. Miller, N. Ebesjer, A. G. Güell, J. V. Macpherson and P. R. Unwin, *Chem. Commun.*, 2012, **48**, 7435-7437.
59 A. G. Güell, K. E. Meadows, P. V. Dudin, N. Ebejer, J. V. Macpherson and P. R. Unwin, *Nano Lett.*, 2014, **14**, 220-224.
60 J. Kim, H. Xiong, M. Hofmann, J. Kong and S. Amemiya, *Anal. Chem.*, 2010, **82**, 1605-1607.
61 I. Dumitrescu, P. R. Unwin, N. R. Wilson and J. V. Macpherson, *Anal. Chem.*, 2008, **80**, 3598-3605.
62 C. B. Jacobs, T. L. Vickrey and B. J. Venton, *Analyst*, 2011, **136**, 3557-3565.
63 S. Sansuk, E. Bitziou, M. B. Joseph, J. A. Covington, M. G. Boutelle, P. R. Unwin and J. V. Macpherson, *Anal. Chem.*, 2013, **85**, 163-169.